Defining a physically accurate laser bandwidth input for optical proximity correction (OPC) and modeling

Ivan Lalovic, Oleg Kritsun[1], Sarah McGowan[1], Joseph Bendik[2], Mark Smith[3], Nigel Farrar

Cymer, Inc., 17075 Thornmint Court, San Diego, CA 92127
[1] Advanced Micro Devices, Sunnyvale, CA
[2] Dynamic Intelligence Inc. (DI [2]), Rancho Bernardo, CA
[3] KLA-Tencor, FINLE, Austin, TX

ABSTRACT

In this study, we discuss modeling finite laser bandwidth for application to optical proximity modeling and correction. We discuss the accuracy of commonly-used approximations to the laser spectrum shape, namely the modified Lorentzian and Gaussian forms compared to using measurement-derived laser fingerprints. In this work, we show that the use of the common analytic functions can induce edge placement errors of several nanometers compared to the measured data and therefore do not offer significant improvement compared to the monochromatic assumption. On the other hand, the highly-accurate laser spectrum data can be reduced to a manageable number of samples and still result in sub 0.5nm error through pitch and focus compared to measured spectra. We have previously demonstrated that a 23-point approximation to the laser data can be generated from the spectrometry data, which results in less than 0.1nm RMS error even over varied illumination settings. We investigate the further reduction in number of spectral samples down to five points and consider the resulting accuracy and model-robustness tradeoffs. We also extend our analysis as a function of numerical aperture and illumination setting to quantify the model robustness of the physical approximations. Given that adding information about the laser spectrum would primarily impact the model-generation run-times and not the run-times for the OPC implementation, these techniques should be straightforward to integrate with current full-chip OPC flows. Finally, we compare the relative performance of a monochromatic model, a 5-point laser-spectral fingerprint, and two Modified Lorentzian fits in a commercial OPC simulator for a 32nm logic lithography process. The model performance is compared at nominal process settings as well as through dose, focus and mask bias. Our conclusions point to the direction for integration of this approach within the framework of existing EDA tools and flows for OPC model generation and process-variability verification.

Keywords: excimer, laser, bandwidth, optical, lithography, focus, resolution, chromatic, aberrations, proximity, illumination, Gaussian, modified Lorentzian

1. INTRODUCTION

The development of high-NA immersion lithography systems and double-patterning integration are enabling continued density scaling of semiconductor devices. As CMOS scaling continues, lithographic variability is emerging as one of the key challenges to realizing the consistent performance gains with each technology node. Furthermore, current device tolerances dictate very stringent patterning control. For example, for the 45nm node, the International Technology Roadmap for Semiconductors (ITRS) [1], roadmap cites a total MPU gate-CD control requirement of 1.9nm (3σ). This requirement is inclusive of all sources of patterning CD variability, including mask CD uniformity, optical proximity correction (OPC) accuracy, as well as exposure tool and resist contribution at all spatial length scales (e.g., intra-field, cross-wafer, wafer-to-wafer and lot-to-lot). At the 32nm node, the ITRS total gate-CD control

Photomask Technology 2008, edited by Hiroichi Kawahira, Larry S. Zurbrick,
Proc. of SPIE Vol. 7122, 71221R · © 2008 SPIE · CCC code: 0277-786X/08/$18 · doi: 10.1117/12.801556

budget is 1.3nm. Given the large number of error contributors, these CD control budgets require sub-nanometer errors for the individual error components.

It is well known that bandwidth variability of the excimer-laser source can also affect CD variability and particularly through-pitch imaging. Thus the characterization, metrology and control of bandwidth in the lithography process has been steadily increasing in importance, particularly for system proximity matching and control of through-pitch imaging.[2-7] Since the introduction of ArF excimer lasers for 193nm lithography, bandwidth stability has improved by more than an order of magnitude supporting imaging at the diminishing depth of focus and increasing numerical apertures across generations of lithography systems. The most advanced dual-chamber lasers based on the master-oscillator power-regenerative-amplifier (MO-PRA) technology feature active bandwidth stabilization, which minimizes variations over life-time and from system to system as shown in Figure 1.

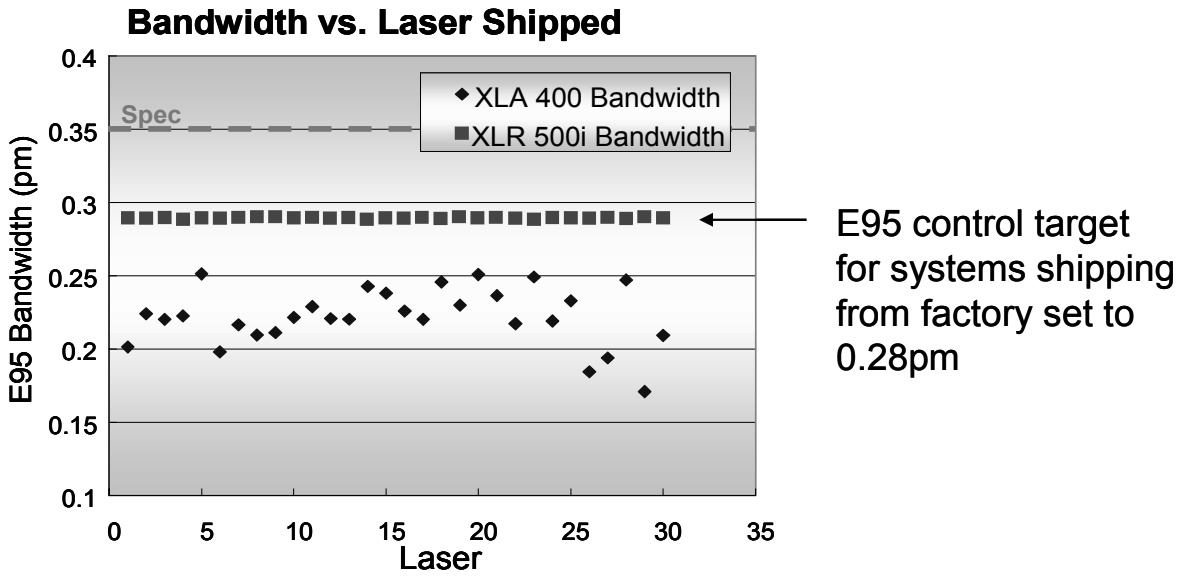

FIGURE 1. Bandwidth of lasers shipping from factory for XLR 500i (featuring active bandwidth stabilization and gas-life extension technology) and XLA 400 systems (without active bandwidth control)

Figure 1 above shows the output bandwidth (in terms of E95) for the first thirty systems shipped from the factory for two generations of dual-chamber lasers. The XLR 500i / XLR 600i immersion laser systems[8] feature active-feedback control techniques to stabilize the bandwidth performance resulting in significant improvement in the uniformity of the laser to laser E95 bandwidth output over the previous generation of laser products. Prior to closed-loop feedback control, improvements in stability were achieved by design and technology that intrinsically reduced variability over lifetime of components and operating conditions. This included improved electrode designs and materials, improved thermal control of the line narrowing module, chamber designs featuring advanced acoustic mitigation and the dual-chamber master-oscillator power-amplifier (MOPA) system configuration.

2. SIMULATION METHODS

PROLITH[9] currently enables direct input of measured laser illumination spectra and features a benchmark full brute-force calculation—allowing input of up to 2024 spectrum data points—as well as numerical speed-up methods for calculating imaging effects using finite laser bandwidth. This capability allows the user to directly determine the speed-accuracy tradeoffs for the given application. Additionally, as of version 9.3.3, PROLITH allows direct input of the laser spectrum and longitudinal chromatic

aberration (rate of defocus with wavelength) via an input text file (*.ILL), which is defined together with other the illumination inputs.

2.1. Lithography Imaging Model for Finite Laser Bandwidth

The effect of finite laser bandwidth is typically modeled as an incoherent superposition of weighted aerial images over a range of defocus values. The defocus values depend on the longitudinal chromatic aberration (LCA), sometimes termed chromatic defocus, which determines the amount of defocus for a given change in wavelength. The image weights at each wavelength value are given by the laser spectrum.

Mathematically, we want to evaluate the following integral in order to obtain the final image intensity $I(x,y,z; f_0)$ at a nominal focus f_0 over the laser spectral distribution $S(\lambda)$ and for a given LCA, described by the slope of the defocus-wavelength relationship, $LCA = \frac{\Delta f}{\Delta \lambda}$, and where x, y, and z are the Cartesian spatial coordinates:

$$I(x,y,z;f_0,S(\lambda)) = \int_{-\infty}^{\infty} I(x,y,z;f_0 - LCA\cdot\lambda)\cdot S(\lambda)\cdot d\lambda \quad \text{(equation 1).}$$

We can express the wafer-plane focus distribution $P(f)$, or focus blur, due to the laser spectrum $S(\lambda)$, by performing the following transformation $S(\lambda_i) \rightarrow P(f_i) = P\left(f_i = \lambda_i \cdot LCA = \lambda_i \cdot \frac{\Delta f}{\Delta \lambda}\right)$.

Therefore, the wafer-plane focus distribution, $P(f)$, is a function of the laser spectrum and the longitudinal chromatic aberration of the projection optics. The LCA value is a constant (over the typical wavelength tuning range of lithography exposure systems) and is determined by the lens material dispersion, refractive power and optical path length, therefore varying for different optical lens designs (or different scanner models). Consequently the same laser spectral output on two different scanner models will scale the width of the wafer-plane focus distribution, $P(f)$, by the ratio of the respective projection optics LCA values. Alternatively, two different laser spectral shapes, $S(\lambda)$, will lead to proportionally different focus distributions on scanners of the same model. The bandwidth of the laser spectrum, whether it be full-width-at-half-maximum (FWHM) or 95-percent-energy-integral (E95%), can be scaled to obtain the width of the wafer-plane focus distribution by,

$$FWHM_{P(f)} = \frac{\Delta f}{\Delta \lambda}\cdot FWHM_{S(\lambda)}, \text{ or } E95\%_{P(f)} = \frac{\Delta f}{\Delta \lambda}\cdot E95\%_{S(\lambda)}.$$

For example, given an LCA of 300nm/pm, a laser bandwidth FWHM of 0.12pm and E95 of 0.26 results in a wafer-plane focus blur FWHM of 36nm and E95 width of 78nm. From our experience, and reported elsewhere in literature,[3,5] the typical range of LCA, values for modern lithography scanners is 200nm/pm to 500nm/pm.

The concept of a focus distribution (focus blur), or focus probability density function, $P(f)$, is useful because in addition to longitudinal chromatic aberration and laser bandwidth, additional distributions of focal positions can arise from sources such as stage tilt (in the direction of the scan), stage vibrations in the z-direction, in addition to in-scan z-position motion of the wafer stage for focus compensation. Mathematically, all of these effects can be included in a cumulative focus distribution $P(f)$ by either straight addition (for the systematic sources such as laser bandwidth, stage tilt and z-scan) or addition in quadrature (for the random errors such as z-vibrations during scan) of the individual distributions. Furthermore, the cumulative focus distribution formalism allows a straightforward way to include any or all of these effects with a single image calculation. We can thus re-write equation 1, more generally:

$$I\left(x,y,z;f_0,P\left(\hat{f}\right)\right) = \int_{-\infty}^{\infty} I\left(x,y,z;f_0 - \hat{f}\right)P\left(\hat{f}\right)d\hat{f} \quad \text{(equation 2).}$$

When evaluating equation 2 above, one can simply approximate the integral with a standard computational algorithm, such as the rectangle rule or Simpson's rule[10], where the interval is broken into discrete steps in focus δf. In this case, the integral is then computed by a direct summation over the

discrete steps in focus. In PROLITH, this approach is available when the main Speed Factor (SF) is set to the value of -1, and the rectangle rule summation step δf is coincident with the available data in the laser illumination spectrum file. This "brute force" approach is useful for detailed calculations where the raw data is evaluated directly. When the main SF is set above -1 (SF>-1), or if no laser spectra are used, a more sophisticated quadrature integration algorithm is used to significantly accelerate the calculation. The accuracy of the final image is dependent on both the main SF approximation setting and complexity of the input illumination spectrum form.

2.2. Modified Lorentzian, Gaussian Fitting and Physical Approximations to the Measured Laser Spectra

In addition to using actual measured laser spectra, the modified Lorentzian (or Cauchy) analytic form has been used to approximate the laser spectrum for the purposes of lithography simulation.[5,11] The modified Lorentzian form is typically expressed as

$$ML(\Delta\lambda) = \frac{(FWHM_{ML})^n}{|2\cdot\Delta\lambda|^n + (FWHM_{ML})^n}.$$

Here, n and $FWHM_{ML}$ are the free fitting parameters that are selected to fit the measured spectrum while $\Delta\lambda$ is the wavelength offset from nominal or peak intensity. The $FWHM_{ML}$ parameter corresponds to the full-width-at-half-maximum of the distribution. The Gaussian analytic form, or a more complex combinations of Gaussian and modified Lorentzian, have also been suggested[12] as refinements of the above that may improve the fitting of modern laser spectra. However, as discussed previously,[13] even the best fits to the measured spectrum data using the modified Lorentzian or Gaussian fail to describe the behavior of real laser spectra particularly in the region of the tails. Although the smoothly-varying analytic forms can reduce the simulation run-time and are simple to use with a parametric representation of the bandwidth and spectral shape, the lithographic imaging differences compared to using physically-measured spectra (through focus and pitch) can be significant. The Gausian form may slightly better fit the measured spectra of current lithography source than the Modified Lorentzian forms, however the errors for both can be on the order of the CD differences induced in going from a monochromatic bandwidth to using a finite bandwidth corresponding to nominal (E95) bandwidths of current light sources. This means that accurate input of laser bandwidth is critical in order to achieve an accurate OPC solution, given the accuracy, model robustness and convergence requirements at the 32nm node.

3. RESULTS

3.1. Down-sampling of the Physical Spectrum Approximations

We have previously described a numerical approximation method,[13] which is based on the physical spectrophotometry measurement of the excimer sources, which results in sub-0.25nm (TIR) residual errors compared to fully-sampled spectra. The resulting physically-based approximations are comprised of 21 to 23 points and have been shown to maintain predictability over a range of pitch and focus settings as well as a range of numerical apertures and illumination conditions. We refer to these sub-sampled spectral inputs as Laser Spectrum Approximations, or LSAs.

The LSA is derived by iterating the sample reduction and background weights to minimize the through-pitch and through-focus CD errors at a specific imaging condition. With 21 to 23-point approximations, the resulting accuracy, compared to using full (>1000-point) measured spectra is on the order of simulator accuracy (sub-0.05nm RMS). Furthermore, the model predictability when applying these inputs to varying numerical aperture, illumination modes and different resist models maintains the ~0.05nm RMS CD residuals through-pitch and focus. In this section we discuss a further reduction in the number of samples and evaluate the trade-offs with model predictability.

Figure 2 below shows the CD differences resulting from a 13-point LSA and a 1000-point factory-measured spectrum of an XLA 300. In this case, the 13-point LSA is optimized for 65nm L/S imaging using c-quad illumination and 1.2NA immersion, with the actual longitudinal chromatic aberration value for a state-of-the art 1.2NA scanner. The 13-point LSA is optimized through a number of iterations until the resulting CD errors at this imaging condition are less than 0.45nm TIR (or 0.075nm RMS).

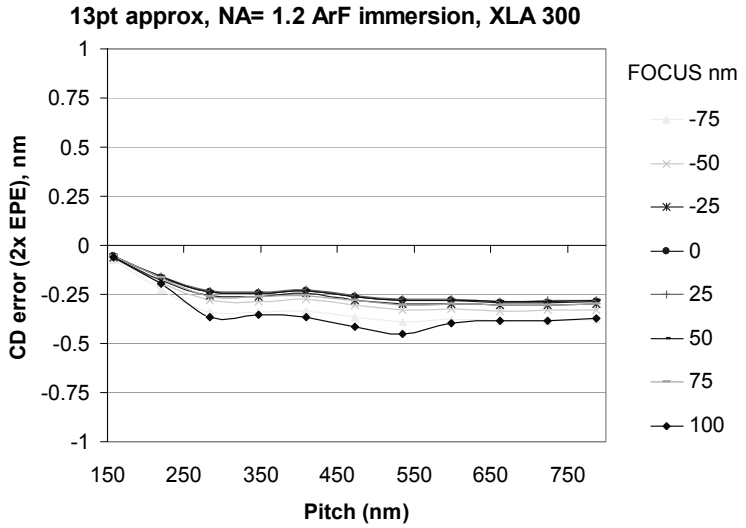

FIGURE 2. 13-point LSA optimized for 1.2NA / c-quad illumination

The number of samples can be reduced even below the 13-points shown previously and still yield an acceptable level of CD residuals. In Figure 3, we show the CD differences between the XLA 300 factory-measured spectrum and a 5-point LSA for the same 1.2NA c-quad imaging condition. Compared to 23 and 13-point LSAs, an increased number of iteration cycles are needed in order to achieve sub-1nm CD errors with a 5-point approximation. Here the through-pitch through-focus CD error range (TIR) is 0.75nm (or 0.125nm RMS). In this case, the 5-point LSA still provides significantly lower CD residuals compared to the use of best-fit Gaussian or Modified Lorentzian forms, which typically range on the order of 1~2nm.

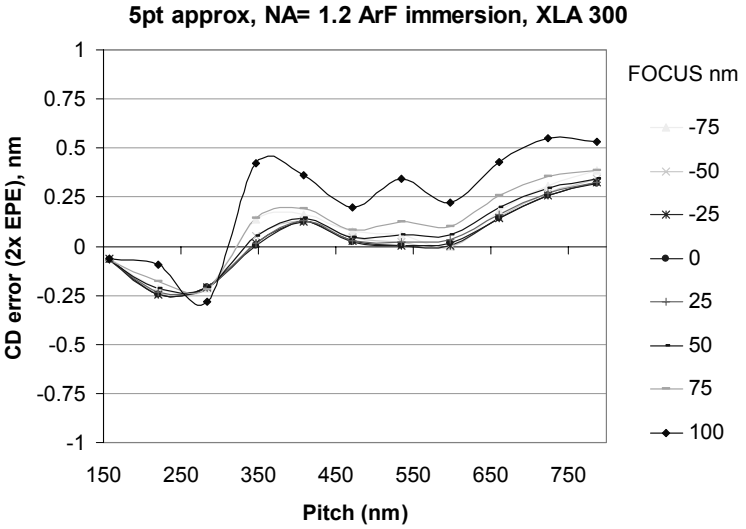

FIGURE 3. 5-point LSA optimized for 1.2NA / c-quad illumination

We further evaluate the robustness of the physical approximations by looking at how the CD residuals behave when the same approximation is applied to different imaging conditions. In Figure 4, we show the through-pitch through-focus CD RMS error for three LSA inputs with 23, 13 and 5 points all optimized at the 1.2NA c-quad condition. We also apply the same LSA inputs to different NA and illumination, without re-optimizing the LSA samples; in this case we chose 0.92NA dry with c-quad illumination and 0.92NA dry and dipole illumination, and compare the CD errors from results obtained using the measured spectra. We see that we can optimize the LSA down to 5-points to maintain a simulation CD error less than 0.2nm RMS for the condition at which the approximation is derived. However, applying the same 5-point LSA to different imaging conditions sharply increases residual errors. Although the sub-sampled (5 or 13-point) approximations could be re-optimized at each of the new settings to minimize the CD RMS their robustness to changes in illumination or imaging are not sufficient. The 23-point LSA on the other hand maintains a constant CD error across a range of imaging conditions. Therefore in order to maximize robustness and therefore model predictability a 23-point LSA seems to provide the best trade-off with computation time. These findings are in agreement with results we reported previously, where we also determined that the 23-point LSA optimized to minimize aerial-image CD errors also maintains sub 0.25nm TIR (or 0.05nm RMS) for full diffusion-reaction resist models.[13]

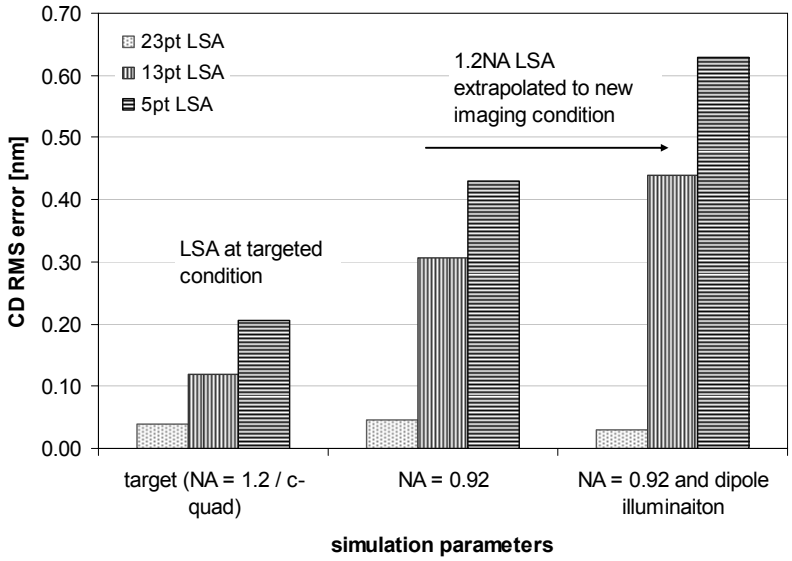

FIGURE 4. LSA model predictability as a function of number of samples

In Figure 5, we summarize the CD accuracy, compared again to the full factory-measured spectra for the XLA 300 laser, as a function of down-sampling different bandwidth model assumptions.

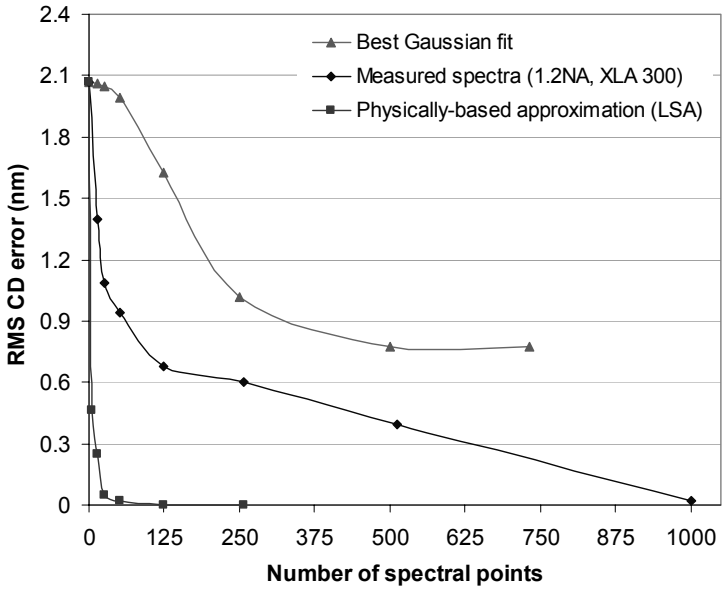

FIGURE 5. Through-pitch & through-focus RMS CD error as a function of the number of samples

As discussed previously, the best Gaussian analytic fit to the factory-measured XLA 300 spectra fails to approach the 1000-point measured input due to the difficulty in matching the intensity in the spectrum tails and the accuracy of the Gaussian does not improve significantly as the number of sampling points are increased. Also, if fixed-interval samples are removed from the 1000-point factory-measured spectra, the accuracy deteriorates gradually down to ~100 samples beyond which the RMS CD error increases more rapidly, quickly approaching the monochromatic CD error (in this case 2.1nm RMS). The accuracy of the LSA spectra seems to saturate at the level of 20 ~ 25-sampling points and further reduction of samples also rapidly increases the CD RMS errors. However, the LSA is re-optimized with each additional down-sampling and the CD RMS errors remain acceptable (~0.2nm RMS) down to 5-points. As discussed previously, reduction in LSA samples below ~20-points comes at the expense of model predictability as a function of other imaging variables.

3.2 Post-OPC Variability in a 32nm Node Logic Process Due to Laser Bandwidth Input

The Modified Lorentzian, or Cauchy, analytic form has been popular among lithographers for defining the laser spectrum in imaging models because it often results in faster simulation run-time (due to symmetry properties of the distribution and the aerial image) and the distribution can be defined with only two parameters (see section 2.2). Many EDA software tools have implemented the Modified Lorentzian input for focus blur and thus optical proximity correction (OPC) can be performed as a function of different Modified Lorentzian inputs. Additionally, post-OPC verification or process variability can be modeled as a function of different bandwidth models to investigate the sensitivity to bandwidth. In Figure 6, we show the results of a 32nm node study of post-OPC process variability where, in addition to different Modified Lorentzian models, the focus, dose and mask CD is systematically varied.

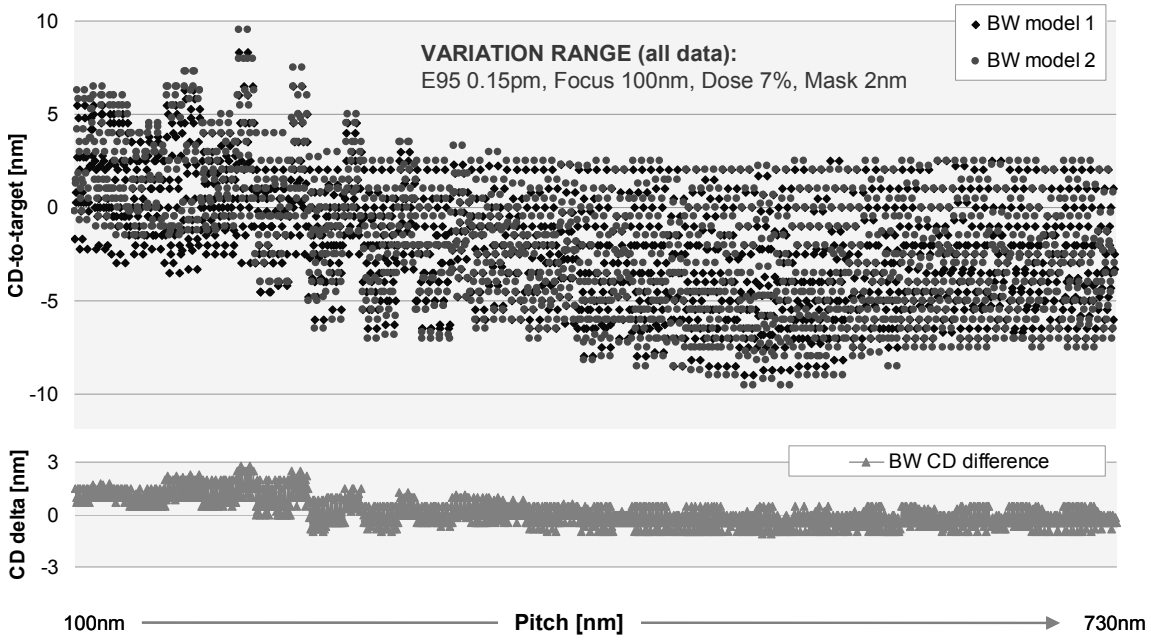

FIGURE 6. Variability modeling of CD-to-target as a function of bandwidth model input together with focus, dose and mask CD error in commercial EDA software

The top graph in Figure 6 shows the CD-to-target error through pitch for all sources of variation considered for the two Modified Lorentzian bandwidth models. The difference between BW model 1 and BW model 2 is simply as difference in values of the FWHM and exponent of the Modeifed Lorentzian function, which span possible differences between two laser types or widely different operating conditions and result in a relative E95 difference of 0.15pm. The lower graph in this figure shows the CD differences between the two bandwidth models over the remaining process variability sources (focus, dose and mask). The maximum CD differences between the two models are as large as 2 ~ 3nm for the critical semi-isolated pitches in this study, therefore pointing to the importance of carefully selecting an appropriate focus-blur model. Furthermore, as we recall from prior comparisons of the best-fit Modified Lorentzian and measured laser spectra (or physical approximations), the modeled CD differences can result in additional errors, which can (in the worst case) be additive to the CD errors of 2 ~ 3nm above.

Figure 7 below shows a subset of the post-OPC variability data discussed previously. The upper graph in this figure shows the CD-to-target errors for the two Modified Lorentzian bandwidth models at best focus and +50nm defocus. We can see here that the BW model 1 (at best focus) has sub-0.5nm CD-to-target errors across the entire range of pitches, which is reflective of the fact that the OPC was performed using this model parameters. For this case, the CD-to-target errors are within the 0.25nm EPE convergence criteria under which the OPC was ran.

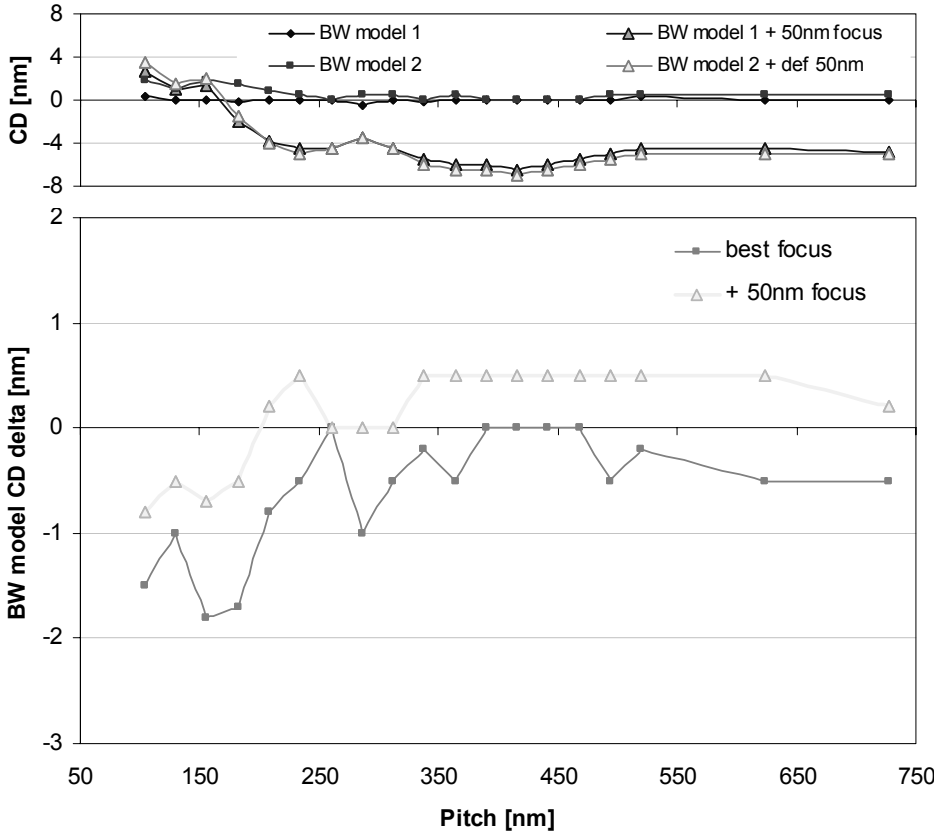

FIGURE 7. a) CD-to-target for two different Modified Lorentzian BW models, and b) CD-to-target differences between the BW models at best focus and 50nm defocus

Although the CD errors increase more significantly with defocus, at best focus, BW model 2 results in errors from target CD as high as 1.5nm for the 100nm pitch features. The through-pitch CD differences between the two laser bandwidth models are shown in the lower graph in Figure 7. In this case the differences between the models are lower when a +50nm focus error is applied, but much of the differences for pitches <300nm are larger than the OPC convergence criteria. The fact that a imaging with a +50nm defocus is needed lower the through-pitch OPC errors between the models, suggests that the bandwidth model differences (and potentially real differences between systems) can be confounded by the best focus setting used for the OPC model generation (or verification) data sets. The potential equivalence between different focus-blur parameters has been discussed previously by Brunner et al.[5]

The BW model CD differences are plotted as a function of dose error in Figure 8. The dose error is varied systematically over a range of +/- 3.5% from nominal. Here we see that the dose bias over the range we evaluated does not change significantly the CD sensitivity as a function of the two Modified Lorentzian models. Therefore, in this case, dose biasing cannot be used to offset the difference between the two laser bandwidth models.

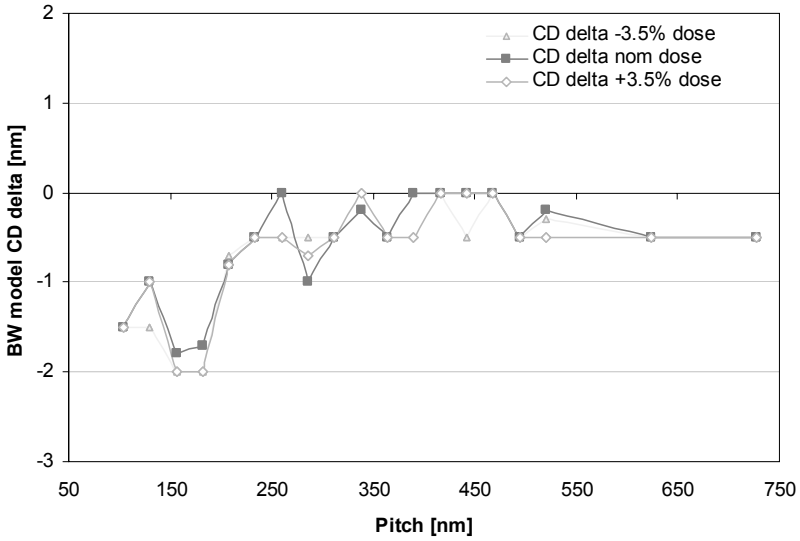

FIGURE 8. CD-to-target differences between the two BW models as a function of +/- 3.5% dose variation

3.3. 32nm-Node Imaging Differences between 5-pt LSA and Modified Lorentzian fit

We additionally simulated the differences between the Modified Lorentzian BW model 2 in the previous section and a 5-point LSA where both were chosen to have the best fit to the same factory-measured laser spectrum. The simulations in this section were carried out using PROLITH, given that the 5-point implementation was not available in the EDA tool we evaluated. Although we use the same imaging condition and actual illuminator profile, here the OPC has not been applied; therefore, the through-pitch CD response is rather different than in previous section. The CD through pitch at best focus is shown in Figure 9 for the monochromatic case (BW E95 = 0), the Modified Lorentzian (BW Model 2 in previous section) and the 5-point LSA.

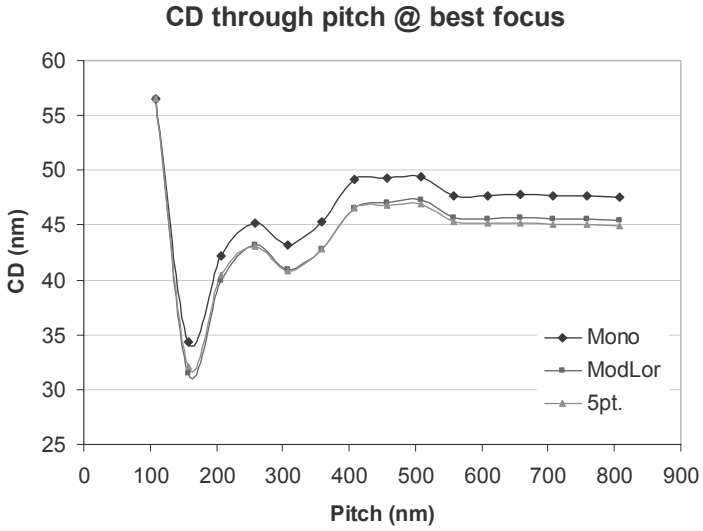

FIGURE 9. CD through pitch for monochromatic imaging, Modified Lorentzian and 5-pt. LSA

In this case the Modified Lorentzian and 5-pt physical approximation show similar behavior through pitch and deviate by as much as 2.5nm from the monochromatic model. The CD differences between the two chromatic models, Modified Lorentzian and 5.-pt LSA, are shown in Figure 10. Here the CD differences are calculated at best focus as well as at 50nm defocus. The CD differences are as large as 1.2nm and

unlike the difference between the two Modified Lorentzians, discussed in the previous section, increase with defocus.

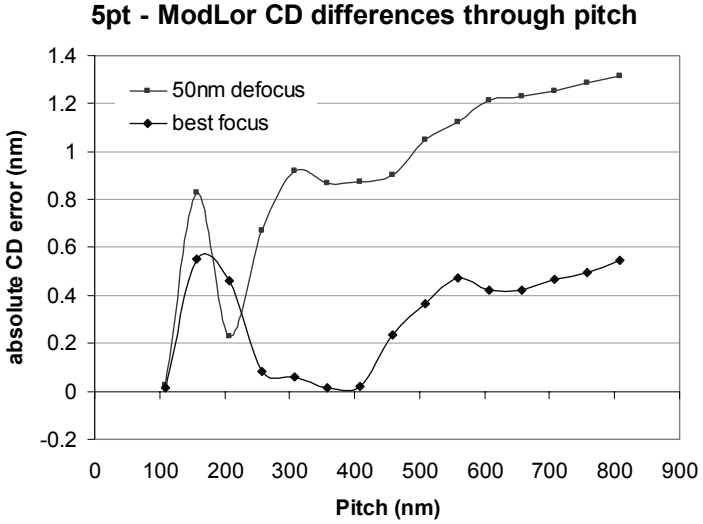

FIGURE 10. Absolute CD difference between a 5-pt physical approximation and Modified Lorentzian fit

4. CONCLUSIONS AND SUMMARY

In this work we have studied the tradeoff between further reduction of samples in the physical laser spectrum approximations and model predictability (or robustness). We find that physical spectrum approximations with less than ~20 sampling points suffer from increasing CD RMS errors through pitch and focus, when the approximation is applied to different imaging settings (numerical aperture or illumination partial coherence) from the condition at which the spectrum is iteratively optimized. Therefore the optimum physical approximation needs to be selected, keeping in mind the trade-off between model predictability and computational cost. For OPC application, given that the LSA approach would only have an impact on the run-time model-generation step, the optimum spectrum sampling may indeed require on the order of 20 ~ 25 points in order to result in most accurate physical representation of the measured laser fingerprint and highest level of approximation robustness.

We also compared an OPC implementation for a 32nm-logic critical-imaging layer, using a couple of Modified Lorentzian bandwidth models. The Modified Lorentzian input can be directly implemented in current EDA software. The differences between the models are on the order of 2~3nm and indicate the importance of accurately defining the focus-blur input. We also compared one of the specific Modified Lorentzian parameter sets to a 5-point physical approximation and additionally observe CD errors of 1nm, therefore the differences between commonly used laser bandwidth inputs at the 32nm node can, in the worst case, result in CD errors of as much as 3 ~ 4nm, which alone consumes more than the available CD budget at these technology nodes. Of course, the magnitude of the errors can in part be mitigated by other process parameters if the mask has already been fabricated, for example by changes in illumination,[14] or is commonly absorbed by the empirical model-calibration step in a typical OPC flow. In either case, the net effect of these errors will result in lowering the overall process robustness and will impact the OPC predictability as is currently being discussed in the industry. Therefore care must be taken to select the appropriate bandwidth model, which most accurately reflects the spectral characteristics of the sources to be used in manufacturing.

ACKNOWLEDGMENTS

The authors graciously thank Robert Rafac and Fedor Trintchouk from Cymer for invaluable discussions of laser spectrometry techniques and data collection, as well as Peter De Bisschop from IMEC for discussion of modeling of laser bandwidth effects.

REFERENCES

1. *International Technology Roadmap for Semiconductors (ITRS)*, 2006 Update, *Lithography Modeling and Simulation*, http://www.itrs.net/reports.html
2. A. Kroyan et al., "Modeling the effects of excimer laser bandwidths on lithographic performance," Proc. SPIE Optical Microlithography XIV **4000** (2000).
3. I. Lalovic et al., "Effects of illumination spectral width on mask error enhancement factor and iso-dense bias in 0.6NA KrF imaging," Proc. SPIE Phot. Tech. Symp. BACUS XXI **4562** (2001).
4. K. Huggins et al., "Effects of laser bandwidth on OPE in a modern lithography tool," Proc. SPIE Optical Microlithography XIX **6154** (2006).
5. Brunner et al, "Laser bandwidth and other sources of focus blur in lithography," Proc. SPIE Optical Microlithography XIX **6154** (2006).
6. Yoshimochi et al, "45nm node logic device OPE matching between exposure tools through laser bandwidth tuning," Proc. SPIE Optical Microlithoraphy XXI **6924** (2008).
7. De Bisschop et al, "Impact of finite laser bandwidth on the CD of L/S structures," *Journal of Micro / Nanolithography, MEMS and MOEMS (JM3)*, **Vol. 7**, No. 3, (2008).
8. V. Fleurov et al, "XLR 600i: recirculating ring ArF light source for double patterning immersion lithography," Proc. SPIE Optical Microlithoraphy XXI **6924** (2008).
9. PROLITH is a registered trademark of KLA-Tencor, San Jose, CA.
10. Press, Teukolsky, Vettering, and Flannery, Numerical Recipes in C, 2nd edition, Cambridge University Press (1992).
11. Lai et al., "Understanding chromatic aberration impacts on lithographic imaging," *Journal of Microlithography, Microfabrication, and Microsystems (JM3)*, **Vol. 2**, No. 2, pp105-111 (2003).
12. R. Rafac, private communication
13. I. Lalovic et al, "Fast and accurate modeling of laser bandwidth for optical proximity correction," Proc. BACUS XXI Photomask Technology Symposium 6730 -66, (2007).
14. N. Seong et al, "Analysis of the effect of laser bandwidth on imaging of memory patterns," to be published at SPIE Lithography Asia, November 2008, Taiwan.